

Redox Activity of Bromides in Carbon-Based Electrochemical Capacitors

Krzysztof Fic,^{*[a, b]} Shinya Morimoto,^[b] Elżbieta Frąckowiak,^[a] and Masashi Ishikawa^{*[b]}

This paper reports on the electrochemical performance of activated carbon electrodes in aqueous solutions of bromide-based species and discusses the results in the broader context of redox-active electrolytes in electrochemical capacitor applications. Operando techniques such as Raman spectroscopy and electrochemical quartz crystal microbalance have been imple-

mented to describe the interactions at the electrode/electrolyte interface. Ex situ experiments, including XPS profiles at different electrode thicknesses, support the discussion by providing insights into surficial and bulk-related processes. Finally, the electrochemical activity of bromides and their advantages and drawbacks are discussed.

1. Introduction

When asked to identify the most important features of an energy storage system of the future, one would definitely say "more energy, more power, less space required and no or negligible performance fade in the long-term". Certainly, all of these features are well-known and highlight the broad spectrum of research challenges currently faced in the electrochemical energy storage field. However, taking into account the various applications (from hybrid or full electric vehicles to personal electronic devices), batteries and electrochemical capacitors (ECs) are the major players in the energy/power storage market.^[1] Certainly, both systems display several advantages and drawbacks, originating mostly from their operation principles. On the one hand, batteries, with their redox-based charge storage mechanism, demonstrate high energy density but suffer from moderate power. Their cycle life is also limited, as the electrode material is exploited during operation. On the other hand, electrochemical capacitors, with their capacitive charge storage mechanism based on electrostatic attraction/repulsion of ions at the electrode/electrolyte interface, deliver high power density accompanied by moderate energy density. Such performance is retained during thousands of charging/discharging cycles, as no redox-based processes occur during operation.^[2–5] Given that, the functional

competition between batteries and capacitors seems to be unreasonable and sometimes artificially induced. Of course, reasonable efforts undertaken to improve energy and power metrics are always well justified, but one should rather not expect that batteries will replace the electrochemical capacitors and vice versa, at least in the nearest future.

It seems that improvements in electrochemical capacitors could bring them closer to batteries in terms of metrics if the specific or volumetric energy is enhanced. This would make the capacitors perfect back-up or short-term energy storage systems to accompany batteries, for instance, under heavy-duty conditions.

The recent development of electrochemical capacitors is oriented towards novel electrode material design,^[6–13] electrolyte formulation,^[9,11,14–22] or identification of the ageing mechanisms aimed at their prevention or inhibition.^[23–32]

To date, activated carbons, with their well-developed surface area, versatile porosity and tunable properties, seem to be the optimal electrode materials in electrochemical applications. As the specific capacitance depends linearly on the electrode/electrolyte interface (of course, until the pore saturation point), the high specific surface area seems to be one of the most crucial criteria. In fact, a high specific surface area results in high specific capacitance values, but one must be aware that the pore distribution must also accommodate the ion dimensions; otherwise, the specific capacitance might be high, but charge propagation will be poor. The majority of activated carbons display a specific capacitance of 100–150 F g⁻¹, reaching slightly higher values in certain cases.^[11,33–37] This is of course well connected with the electric double-layer capacitance, reaching a maximum of 50 µF cm⁻².^[11] Considering that the currently available electrolytes display stability up to 3.5 V on activated carbon electrodes,^[38] the maximum energy output for a symmetric device does not exceed 60 Wh kg⁻¹ *ceteris paribus*.

Since the energy *E* stored in the capacitor depends on the capacitance *C* and the operating voltage *U*, $E=0.5CU^2$, increasing the capacitance seems to be a reasonable approach for energy improvement. One should keep in mind that the capacitance value increase does not mean that the intrinsic

[a] Dr. K. Fic, Prof. E. Frąckowiak
Poznan University of Technology
Institute of Chemistry and Technical Electrochemistry
Berdychowo 4, 60-965 Poznań, Poland
E-mail: krzysztof.fic@put.poznan.pl

[b] Dr. K. Fic, Mr. S. Morimoto, Prof. M. Ishikawa
Kansai University
Department of Chemistry and Materials Engineering
Faculty of Chemistry, Materials and Bioengineering
3-3-35 Yamate-cho, Suita 564-8680, Japan
E-mail: masaishi@kansai-u.ac.jp

Special Collection An invited contribution to a Special Collection on Electrolytes for Electrochemical Energy Storage

© 2020 The Authors. Published by Wiley-VCH Verlag GmbH & Co. KGaA. This is an open access article under the terms of the Creative Commons Attribution License, which permits use, distribution and reproduction in any medium, provided the original work is properly cited.

capacitance of the electric double layer could be modulated. In fact, higher capacitance values result from merging the capacitive and redox-based charge storage mechanisms. This effect, called pseudocapacitance, is quite often confused with typical redox-based storage currently. It is worth highlighting that initially, only certain transition metal oxides, such as MnO_2 and RuO_2 , or electroactive polymers, such as polyaniline, have been claimed to be pseudocapacitive.^[39] Recently, the term ‘pseudocapacitive’ has developed in an uncontrolled manner, but in fact, the principles did not change.^[40–41] Enormously high capacitance values, quite often exceeding 500 F g^{-1} , claimed for NiO , Fe_2O_3 or other redox-based materials should induce eyebrow raising rather than scientific “excitation”. Such values are quite often accompanied by incorrect specific energy

estimation, where the values approaching the characteristics of Li-ion systems are also claimed. As already mentioned, for symmetric EDL-based systems operating with ionic liquids ($U_{\max}=3.5 \text{ V}$), the specific energy of the device should not exceed $60\text{--}70 \text{ Wh kg}^{-1}$, as presented in Figure 1A.

It must be said that one is allowed for the energy estimation on the single electrode basis only in the case of symmetric device, i.e., when the specific capacitance values for both electrodes are identical. In this case, the specific energy of the cell is expressed by the formula $E=0.125 C_{\text{electrode}} U_{\max}^2$.

For any other case, the specific energy must always be calculated on the basis of total cell capacitance and the mass of two electrodes. This situation is represented in Figure 1B. This graph clearly shows that to approach the Li-ion systems (at

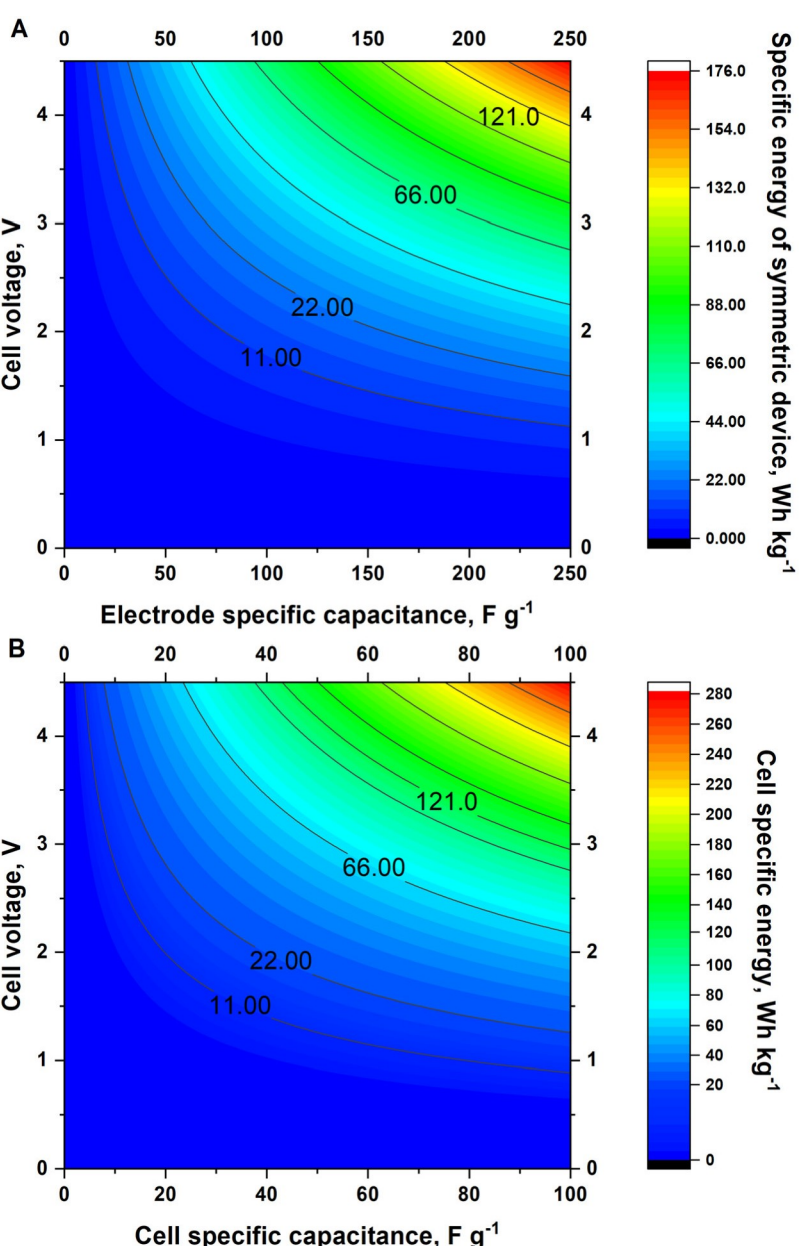


Figure 1. Specific energy values calculated at certain electrode capacitance and cell voltage values (A) and calculated from the total cell capacitance (B) for symmetric EC devices.

least 120 Wh kg⁻¹), one should ensure a cell capacitance of 80 F g⁻¹ and a cell voltage of at least 3 V. With typical capacitive storage, such criteria might be very difficult to meet. It should be mentioned that both calculations are based only on the mass of electrode materials, whereas for real systems, the mass of electrolyte, separators and cases must be included, resulting in energy values approximately 3 times smaller.

Redox-active electrolytes appeared to be a very promising solution aimed at increasing the total capacity. Relatively slow solid-state kinetics of metal oxides have been “replaced” here by much faster redox reactions at the electrode/electrolyte interface, originating from electrolyte solution. Initially, bromine-based compounds were proposed as a source of redox-based capacity in organic media^[42–44] and iodine-based in aqueous media.^[45–46] These works have been followed by studies by other researchers, proposing several other redox-active compounds and demonstrating redox activity in electrolyte solutions, such as hydroquinone, ethyl viologen, methylene blue or thiocyanates.^[10,19,21,47–57] Grafted anthraquinones displaying similar performance might also be considered in this family.^[58–60]

In this paper, we report on the electrochemical performance of a carbon-based electrochemical capacitor operating with a redox active electrolyte based on a bromide/bromate redox couple in an aqueous electrolyte. The motivation for this study was the relatively high oxidation potential of the Br⁻ specimen, which might be beneficial for the total cell voltage and capacitance but harmful for the carbon electrode during long-term operation, as it has been reported that carbon oxidation might occur even below the water decomposition voltage.^[23–24,61] In fact, initial work demonstrating the application of KBr as a redox-active agent confirmed that the redox activity of Br⁻ is observed at rather elevated capacitor voltages.^[62] This might cause the carbon surface to be prone to surficial oxidation and capacitance fade. Moreover, BrO₃⁻ is expected to be reduced during capacitor operation and to stimulate Br₂ generation. Thus, the paper provides insight into the positive and negative aspects of aqueous, bromide-based electrolytic solutions as electrolytes for electrochemical capacitors.

Experimental Section

All chemicals (KBr, KBrO₃) were of ACS® grade and were purchased from Sigma-Aldrich® (Poland). No further treatment was performed. To obtain 1 mol L⁻¹ KBr and 0.05 mol L⁻¹ KBrO₃ solutions, appropriate amounts of the respective salts were dissolved in deionized water. For the mixed solution, i.e., 1 mol L⁻¹ KBr + 0.05 mol L⁻¹ KBrO₃, appropriate amounts of the respective chemicals were placed together in a volumetric flask, and deionized water was added to the flask volume.

Activated carbon electrodes were made of two different carbon materials: self-standing activated carbon cloth ACC 507-20 from Kynol® (Japan) and activated carbon powder YP-80F from Kuraray® (Japan). In the case of the ACC 507-20 material, disk-shaped electrodes with an average mass of 9.5 mg and a geometric surface area of 0.785 cm² were cut. For the *operando* Raman experiments,

an electrode with a diameter of 5 mm and geometric surface area of approximately 0.2 cm² were used.

To obtain the composite electrode from powdered activated carbon (YP-80F), 10 wt.% poly(vinylidene fluoride) and 5 wt.% carbon soot C65 (provided by Timcal®, now Imerys Graphite & Carbon, Japan) were added to the powder and homogenized in acetone until solvent evaporation. Then, the electrodes were pressed under 10 MPa for 60 s on a hydraulic press in a designed cell, formulating disk-shaped electrodes of approximately 9 mg and 0.785 cm² of geometric surface area.

If not stated otherwise, the electrochemical measurements refer to the composite electrode made from Kynol® ACC 507-20.

Nitrogen adsorption isotherms (77 K) were recorded with an ASAP 2460 instrument (Micromeritics, USA) to estimate the specific surface area of the carbon materials. Pore size distributions (PSDs) have been estimated with the 2D NL-DFT model.^[63–64]

Ion size calculations were performed with Gaussian®09 W software using the DFT model and the ground state method. The B3LYP functional and 6-31G basis set were used. To approximate the size in aqueous solution, the IEFPCM solvation model was used.

Operando Raman spectra were recorded with a DXR Raman microscope (ThermoFisher®, USA). A laser wavelength of 622 nm with 5 mW power was used.

XPS spectra were recorded with a JPS-9010MC (JEOL Ltd., Japan) instrument with an X-ray wavelength of 0.989 nm (1252.6 eV, Mg-K α). Ar etching of the electrode surface was performed to investigate the changes in the electrode bulk.

All electrochemical tests – cyclic voltammetry, galvanostatic charging/discharging and electrochemical impedance spectroscopy – were recorded with a VMP3 multichannel potentiostat/galvanostat (BioLogic, France). Electrochemical quartz crystal microbalance profiles were recorded with a Seiko 922 instrument (Seiko®, Japan) connected to a VMP3 electrochemical instrument. The coating was drop-cast on a quartz crystal resonator (9 MHz) with gold current collector with mirror-like finish. The slurry was obtained by dissolving the activated carbon powder (YP-80F) in PVdF solution (used as binder, 50 wt.% in NMP as a solvent) with a final composition of 80 wt.% activated carbon and 20 wt.% binder. During the experiment, the resistivity measured by EQCM did not change by more than 2%.

In the three-electrode cell, the oversized activated carbon electrode (approximately 10 cm²) served as the counter electrode, while a saturated calomel electrode (SCE) was used as the reference electrode.

For the three-electrode setup, the capacitance values are expressed per electrode. For the full cells, the capacitance is expressed per total active mass in the cell. For the galvanostatic profiles, the capacitance has been calculated from the integration of the curve.^[65]

2. Results and Discussion

Nitrogen adsorption at 77 K confirmed that both materials are microporous and have similar specific surface area values and pore size distributions (Figure 2).

Taking into account the pore size distribution, both carbons seem to be suitable for accommodating the Br⁻, Br₃⁻ and BrO₃⁻ anions. Such a selection of the species is based on the expected

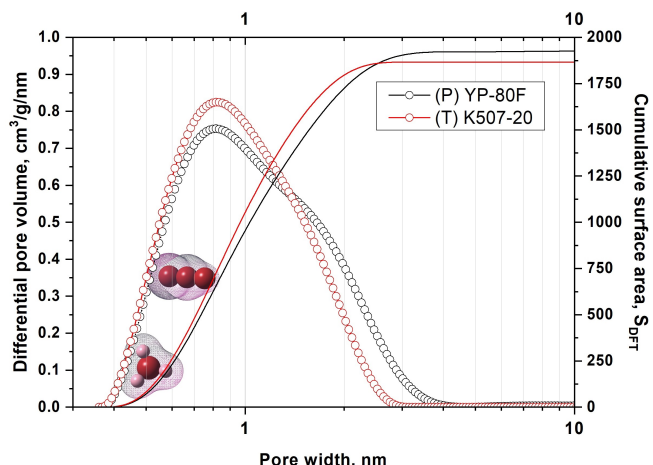


Figure 2. Pore size distributions and cumulative surface area for the activated carbons used for the electrode formulation. BrO_3^- and Br_3^- are placed in the respective pore size range.

electrolyte pH and the predominance area of ions, predicted from the Pourbaix diagram (Figure 3).

Pourbaix diagram has been calculated for the temperature of 25 °C, taking into account the respective concentrations and solubility of KBr and Br_2 . In this context, one should keep in mind that the temperature might affect both, the concentration of the redox-active species, as well as their redox potentials. Preliminary studies, accompanied by theoretical calculations for the temperatures ranging from 10 °C to 60 °C suggest that the temperature impacts mostly the equilibrium between Br_3^- and Br_2 , with the preference towards Br_2 . This means that the reversibility and efficiency of the charging/discharging process might be aggravated. Taking into account the redox kinetics, one should be aware that the reaction rates might improve with temperature, but on the other hand, parasitic processes (including corrosion, self-discharge and leakage currents) will increase as well.

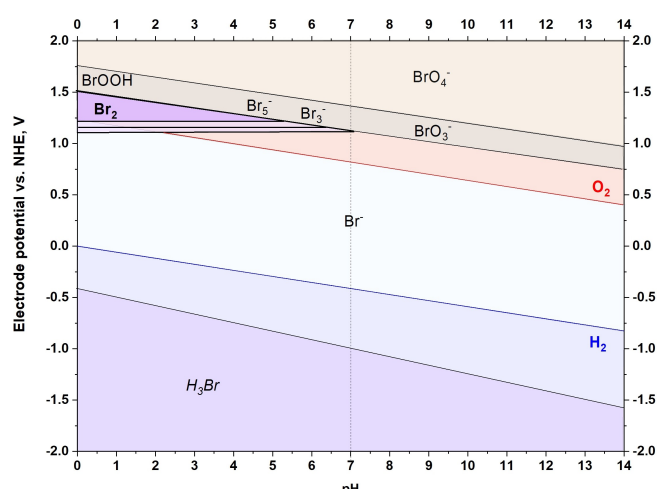
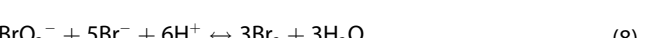
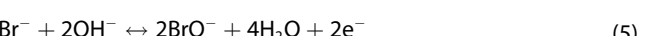


Figure 3. Pourbaix diagram for bromine and related species in aqueous solution at 25 °C. Equilibrium potential lines correspond to Br^- concentrations of 1 mol L⁻¹ and BrO_3^- concentrations of 0.05 mol L⁻¹. Based on.^[66]

It seems that to benefit from the rich redox chemistry of bromine-based species, one should maintain the electrolyte pH below 7, as bromine (Br_2) and polybromides (Br_3^-) might only be formed at such pH values. These processes can be described by the following reactions [Eqs. (1)–(8)]:



For the electrolytes investigated in the study, pH ranged from 5.8 to 6.1. For pH values higher than 7, oxidation of Br^- results in direct BrO_3^- formation; notably, the solubility of bromate-based species is moderate, and the precipitation of solid KBrO_3 might occur. It has been determined that the maximum concentration of KBrO_3 under the experimental conditions is 0.38 mol L⁻¹. Thus, alkaline pH should be avoided as far as long-term operation at elevated voltages is foreseen. Buffer-like solutions might be considered in order to maintain the pH value during long-term operation, essentially at elevated voltages, as the hydrogen evolution might generate local pH changes towards higher values.

Another important information delivered by Figure 3 is the fact that for electrolyte pH values above 3, the oxygen evolution reaction might theoretically precede Br_2 and Br_3^- formation. In such a case, electrode oxidation and an increase in internal pressure are very likely to occur.

Interestingly, Br^- seems to be quite stable under cathodic conditions, which might suggest a high hydrogen evolution overpotential.

In fact, cyclic voltammetry recorded in a three-electrode cell at a 5 mV s⁻¹ scan rate confirmed these findings (Figures 4A–D).

Figure 4A represents the cyclic voltammetry profile for the AC electrode operating with 1 mol L⁻¹ KBr aqueous solution in three-electrode cell. The capacitive properties are maintained within a wide potential range, exceeding even the hydrogen evolution potential. The average specific capacitance measured by the integration of the CV profile ranged from 98 to 121 F g⁻¹ (14 mAh g⁻¹ for 0.5 V of the potential window, 41 mAh g⁻¹ for 1.25 V of potential window). Interestingly, at low cathodic values, hydrogen electrosorption is observed. Up to –1.4 V vs. NHE, the hysteresis loop on the current profile and the oxidation peak (from –0.5 to +0.5 V vs. NHE) suggest that this process is reversible. Reversibility was evaluated and quantified according to protocols proposed by Xu and Kötz.^[67–68] For higher values, i.e., up to an electrode potential of –0.3 V vs.

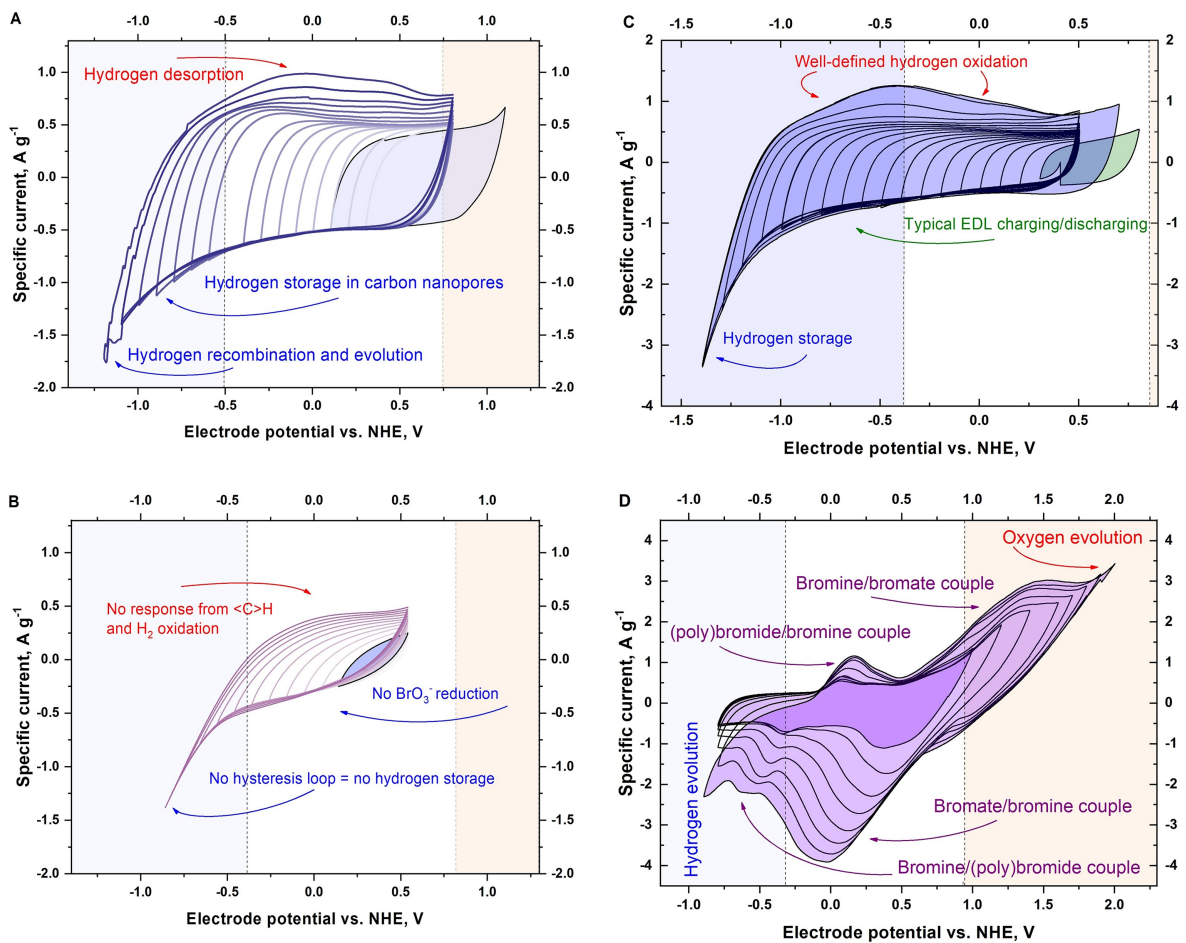


Figure 4. Cyclic voltammetry profiles for activated carbon electrodes operating in various bromide-based solutions: A) 1 mol L^{-1} KBr, B) 0.05 mol L^{-1} KBrO_3 , C) 1 mol L^{-1} KBr + 0.05 mol L^{-1} KBrO_3 for freshly soaked electrodes, and D) 1 mol L^{-1} KBr + 0.05 mol L^{-1} KBrO_3 after anodic polarization. Theoretical hydrogen and oxygen evolution potentials indicated as coloured zones were determined on the electrolyte pH values.

NHE, the S-value does not exceed 0.02 value. Deeper cathodic polarization, i.e., up to a potential of -0.9 V vs. NHE, makes the S-value slightly higher (0.05–0.08). For potentials greater than -0.9 V vs. NHE, the S-value reaches 0.09–0.11. This has been assumed as a practical potential limit for reversible hydrogen storage, as for more cathodic potentials, S-value indicated inefficiency between charge provided and received. S-values lower than 0.1 for scans exceeding hydrogen evolution potentials means that reversible hydrogen electrosorption could contribute as a pseudocapacitance source on the negative electrode, balancing the expected capacity increase on the positive electrode. However, for the last scan, some perturbations of the current profile might be observed; this is most likely caused by the gaseous hydrogen (H_2) evolving from the electrode surface. Furthermore, the shape of the current profile at the cathodic vertex potential also suggests that a portion of the hydrogen might be adsorbed on the electrode surface. Thus, such deep cathodic polarization must be avoided in a full device, since gas generation will certainly result in an internal pressure increase.

It should be mentioned that in Figure 4A, redox activity of Br^- is not observed. One should be aware that in this case, the

electrode was polarized towards cathodic potentials from the initial so-called rest potential. This has been done to evaluate the stability limit of the negative electrode, as it has been shown in previous studies that alkali-metal redox activity might aggravate hydrogen electrosorption.^[69] However, a small increase in the recorded current for the CV with vertex potential at $+1.1 \text{ V}$ vs. NHE suggests the initial oxidation of Br^- . For this scan, the S-value was of 0.13.

To verify the performance of the carbon electrode in the presence of BrO_3^- , cyclic voltammetry (5 mV s^{-1}) was recorded in the electrolyte concentrated at 0.05 mol L^{-1} . Resistive CV characteristics most likely result from the low concentration and poor conductivity of the electrolytic solution (approximately 30 mS cm^{-1}). The specific capacitance is low (approximately 40 F g^{-1} , i.e. $\sim 6 \text{ mAh g}^{-1}$ for 0.5 V of potential range). One should note the lack of hydrogen storage in this solution – there is no hysteresis loop at cathodic potentials, and no hydrogen oxidation peak could be observed. High inefficiency has been also reflected by S-values higher than 0.2 for scans exceeding hydrogen evolution potential. Again, within the stability region, no indication for bromate activity could be observed. This suggests that the BrO_3^- anion is also stable

under the experimental conditions and will not impact the negative electrode performance.

Since it seems to be difficult to induce the redox chemistry of bromide-based species within the water stability region in an almost neutral electrolyte (as predicted from the Pourbaix diagram), an electrolyte containing both forms – Br^- and BrO_3^- – has been prepared and examined. This concept exploits the possibility of generating Br_2 once bromide and bromate anions are in the common solution. This might have a benefit in terms of generating redox activity, without approaching oxygen evolution potential and subjecting the carbon electrode to oxidative conditions. The results are presented in Figure 4C and 4D.

Again, once the electrode is polarized towards cathodic potentials from the rest potential, no significant redox activity of bromides can be observed (Figure 4C). However, the specific capacitance is higher and reaches 138 F g^{-1} (calculated from the CV integral). This might result from the higher concentration of ions in the electrolytic solution. Moreover, current hysteresis confirms that hydrogen storage occurs after exceeding its evolution potential. The broad oxidation peak confirms that the process is reversible and should not affect the charging/discharging efficiency in a full device unless recombination (e.g., Tafel reaction) occurs. In this case, the efficiency was also verified by S-value testing and for the double-layer storage it demonstrated the values lower than 0.05, for potential values higher than -1.0 V vs. NHE -0.11 , then for values lower than -1.3 V vs. NHE -0.08 .

These results confirm that the presence of bromide-based species in the electrolytic solution does not aggravate hydrogen electrosorption, contrarily to the presence of iodides.^[69]

Polarization towards anodic potentials (Figure 4D) demonstrates the redox activity of bromine-based species. The presence of BrO_3^- induced Br_2 generation below oxygen evolution potentials; therefore, one should assume that in such potential ranges, the carbon electrode is protected against oxidation. Further polarization towards anodic potentials results in the recorded current increase and demonstrates a multistep (and multiproduct) redox process. It should be noted that the theoretical oxygen evolution potential is exceeded, and no significant oxygen evolution (supposed to be irreversible) is observed. Small deteriorations and an increase in the current profile at potentials higher than $+1.5 \text{ V}$ vs. NHE suggest that oxygen starts to be formed at that potential value. Unfortunately, the most likely multielectron redox process of bromine-based species results in a broad redox peak with the reduction peak maximum shifted by almost 1.0 V. In this case, the energy efficiency of the capacitor might be seriously affected. However, such information indicates that the positive electrode potential should not be maintained at elevated values. Additionally, it would be difficult to balance the charge by the negative electrode, as hydrogen storage does not provide enough charge.

To verify the reversibility of the bromide-based processes, an electrochemical quartz crystal microbalance was employed. The activated carbon electrode coated on the 9 MHz resonator was subjected to cyclic voltammetry scan within the same

potential range as presented in Figure 4D. We are aware that direct recalculations of the frequency changes to the mass changes and evaluation of the species at the interface might be incorrect at such electrolyte concentrations; therefore, we discuss the ‘relative’ change only.^[37,70–73]

As shown in Figure 5, during the initial scans, the mass of the electrode changes substantially, and it appears that some sorption occurs. Interestingly, this specimen does not dissolve during reversed polarization, although the electrochemical response (current profile) does not change considerably. It has been assumed that Br_2 could be responsible for such a result, as it accumulates during subsequent scans. Taking into account the dynamic conditions as well as good solubility of Br_2 (i.e., $\sim 0.21 \text{ mol L}^{-1}$, i.e., much higher than that for iodine, $0.0013 \text{ mol L}^{-1}$), partially dissolved Br_2 might further react with Br^- and result in Br_3^- generation. The occurrence of higher polybromides (e.g., Br_5^-) cannot be excluded; however, at electrolyte pH (~ 5.3), their presence might be doubtful.

Operando Raman experiments (Figure 6), performed for the activated carbon electrode from -0.75 V vs. NHE to $+1.75 \text{ V}$ vs. NHE potential values, confirmed that the carbon electrode undergoes an initial charge transfer process and then remains stable, even at elevated potentials.

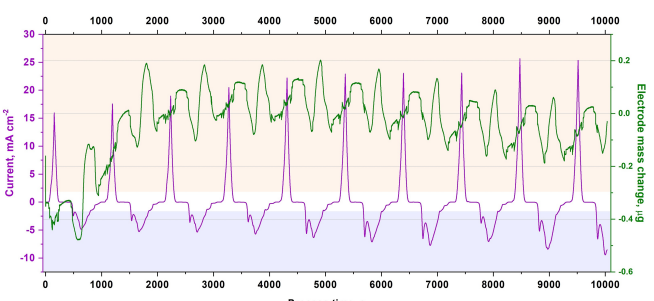


Figure 5. Electrochemical quartz crystal microbalance profiles for the activated carbon electrode with the frequency change recalculated to the electrode mass change. A 9 MHz resonator was covered by a thin activated carbon layer with an electrolyte of $1 \text{ mol L}^{-1} \text{ KBr} + 0.05 \text{ mol L}^{-1} \text{ KBrO}_3$.

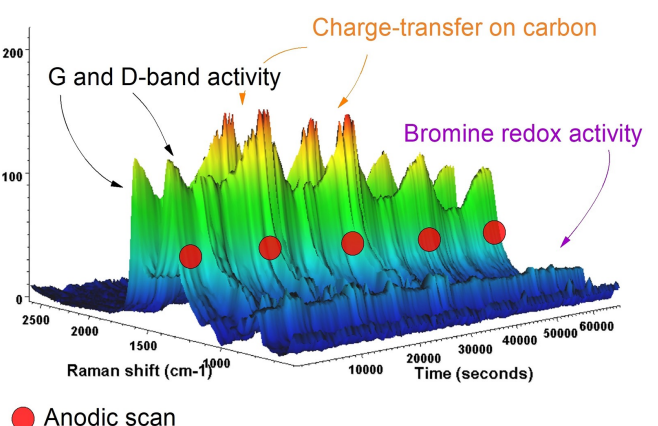


Figure 6. *Operando* Raman spectra for the activated carbon electrode operating with the electrolyte $1 \text{ mol L}^{-1} \text{ KBr} + 0.05 \text{ mol L}^{-1} \text{ KBrO}_3$.

The Raman response reflects activated carbon electrode (and electrolyte) performance similar to that of the EQCM. Initially, the intensity of the so-called D and G Raman bands (approximately 1300 and 1500 cm^{-1}) at the positive vertex potentials increases, that might indicate the contribution of carbon in the charge storage process. The kind of charge transfer (surface oxidation, generation of defects, etc.) cannot be directly determined, as the electrolyte impacts the spectra remarkably. However, a maximum of the Raman intensity is recorded for the next scans (2^{nd} and 3^{rd}). It must be said that the increase in the D and G band intensities cannot be directly translated to the charge transfer process, as their spectral origin is more than complex. In this context, we refer to other reports that provide insightful remarks on the *in-situ* Raman observations for various carbon-based materials.^[74–80] In the case of our study, we assume that it is most likely related to the formation of either Br_2 or $-\text{Br}$ bonds, as the intensity typical of bromine, recorded at Raman shifts of up to 500 cm^{-1} changes accordingly. Certainly, oxidation of the carbon surface cannot be neglected, as the shoulder on the D band appears at Raman shifts of 1100 – 1300 cm^{-1} . However, this shoulder disappears during the negative scan; in such a case, one can assume redox activity of quinone-hydroquinone functional groups, generated by (mild) oxidation of the carbon surface.^[76]

XPS results, presented in Figure 7, confirm the findings from Raman spectroscopy measurements. To obtain comprehensive insight, 4 samples were investigated: pristine electrodes, electrodes immersed only in the electrolyte and positive and negative electrodes after long-term cycling.

One must be aware that the results from *operando* Raman and ex situ XPS cannot be directly compared; however, some common conclusions might be drawn.

Primary XPS regions for 5 elements were surveyed: C1s, O1s, N1s, Br3d and Fe2p. Furthermore, to investigate the change in the element content along the electrode thickness, Ar etching (sputtering) was performed for 1 s, 5 s, 10 s, and 30 s after collecting the data for the sample surface.

The C1s spectra of the pristine electrode confirmed that the sample surface is composed mostly of sp^2 carbon, as the peak is centred at 284 eV . For the initial scan, some shoulder centering at 284.8 eV might suggest the presence of the C-sp³ form on the surface. This might result from the slight oxidation of the carbon surface and is in good agreement with the O1s spectra, which also indicate the presence of certain oxygen forms at the surface. It seems that the carbon functional groups are composed mostly of C=O (289 eV for C1s and 532 eV for O1s) and C—O (287 eV for C1s and 533 eV for O1s) components. Taking into account the C-O=C band activity at 288.5 eV on the C1s spectrum, one might assume the presence of ester-based groups. The presence of oxygen has been confirmed for all scanned surfaces; however, the O1s relative intensity decreases together with the increase in C1s intensity; therefore, surficial oxidation is assumed. No remarkable signal for Br3d or N1s was recorded.

For the sample soaked in the electrolyte, the recorded spectra are similar to those of the pristine electrode, apart from the Br3d region. It seems that bromide anions likely react with the carbon surface and thus might be seen in the XPS spectra.

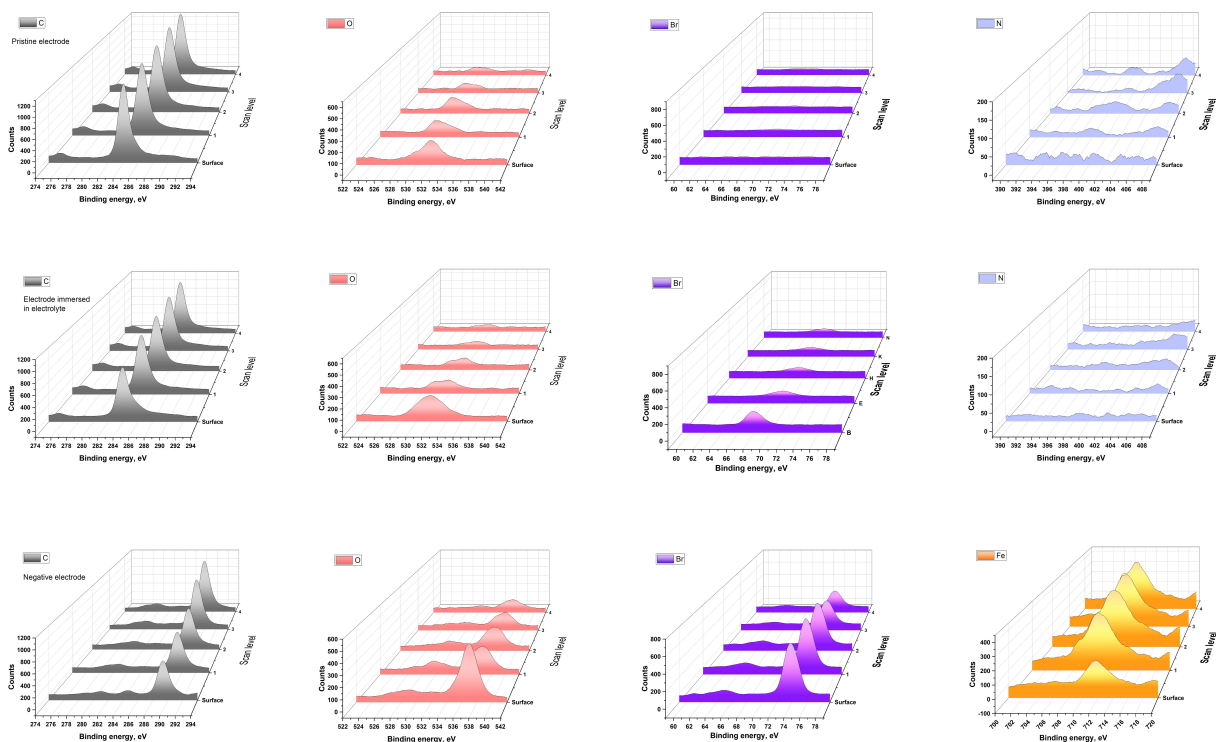


Figure 7. XPS spectra of pristine carbon and carbon immersed in the electrolyte and for the positive and negative electrodes of the capacitor operating with $1\text{ mol L}^{-1}\text{ KBr} + 0.05\text{ mol L}^{-1}\text{ KBrO}_3$ electrolyte subjected to long-term cycling at 1.8 V .

However, since no polarization was applied, the reaction occurred mostly on the surface, as the relative intensity decreased for the next layers. As expected, no N1s was observed. One should, however, note that there is a remarkable change in contribution to the O1s peak between pristine sample and the sample immersed in electrolyte: it seems that the sample immersed in the electrolyte displays the oxygen contribution mainly in the C–O region (533 eV for O1s), while the pristine electrolyte displays this contribution in the C=O region (531 eV for O1s).^[81] This might suggest slightly oxidative properties of the electrolyte solution; however, one should also note that the solution has not been degassed prior to the experiment, and it might also be the impact of the O₂ dissolved in the electrolyte.

Quite interesting results have been obtained for electrodes subjected to long-term cycling. For the negative electrode, the C1s spectra show increasing carbon content on the surface, with no remarkable change in the shape vs. pristine material or the electrode immersed in the electrolyte. The shift in the spectra most likely originates from the lower conductivity of the sample. One could also assume the deposition of K₂CO₃, as the MeCO₃ band for C1s is observed at 288–290 eV.^[82] Then, for the O1s scans, it appears that the highest oxygen content is recorded for the surface and then remarkably decreases to a level comparable to that of the sample immersed in the electrolyte. However, the peaks recorded in this region are quite symmetric, which might suggest an equal contribution from the C–O and C=O functional groups. This was somehow surprising, since oxidation of the electrode was not expected on the negative side; however, one should not ignore the fact that BrO₃[–] might precipitate (KBrO₃) and amplify the signals from both oxygen and bromide. To some extent, this would be in good agreement with the results observed for the Br3d region, where an almost constant concentration of Br species is observed. Notably, elemental Br (Br₂) is normally not detected by XPS measurements. An Fe2p region survey spectrum demonstrated that there is also remarkable Fe₂O₃ content on the electrode surface. The content increases with the scanning depth; however, it could be assumed that the surficial layer has been removed before washing the sample prior to XPS measurement.

The results obtained for the positive electrode suggest quite remarkable changes in the electrode structure. The relative intensities for C1s are significantly lower than those for pristine carbon; however, they are not shifted towards high eV values; therefore, no changes in conductivity are assumed. The spectra for the O1s region demonstrate a high contribution from oxygen to the overall composition of the electrode surface, but the partial contributors (C–O or C=O) seem to change from the surface to the electrode bulk. Again, C–O is assumed with the electrode matrix, as both C–O–C (~286 eV for C1s and 533 eV for O1s) are amplified. Scans in the Br3d region confirm the presence of Br-based species, with decreasing intensity along the electrode thickness. Again, a high Fe₂O₃ content has been found, which might be detrimental to long-term cycling, as the carbon porosity might become clogged or

the current collector might undergo remarkable corrosion. This aspect will be verified later.

These results obtained in the three-electrode cell need to be verified in the full cell.

The galvanostatic charging/discharging profile recorded for the full cell equipped with the reference electrode and corresponding cyclic voltammetry characteristics are presented in Figure 8A–B.

The galvanostatic profile presented in Figure 8A confirmed the capacitive charge storage mechanism at the full cell. A maximum voltage of 1.8 V was achieved at a current density of 1 A g^{–1}. At higher voltages, the system demonstrated high energetic inefficiency and an enormous ohmic drop, which might be related to extensive hydrogen evolution on the negative electrode.

However, individual potential profiles reveal a typical hybrid charge storage mechanism: the negative electrode operates in a very broad potential range (from –1.0 to +0.5 V vs. NHE), while the positive value demonstrates a very high capacity and a very narrow operating potential range. Since the terminal potential values refer to 1.8 V of the capacitor voltage, it seems

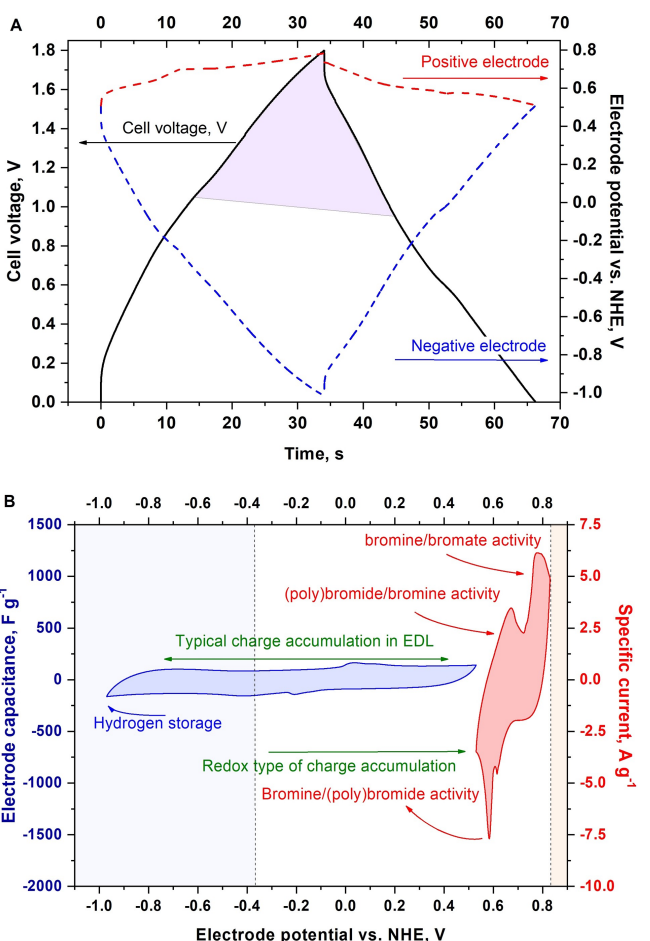


Figure 8. A) Galvanostatic charging/discharging profile (1 A g^{-1}) and B) cyclic voltammetry at 5 mV s^{-1} profile for the full cell operating with a 1 mol L^{-1} $\text{KBr} + 0.05 \text{ mol L}^{-1}$ KBrO_3 electrolyte. Theoretical hydrogen and oxygen evolution potentials are indicated as coloured zones based on the electrolyte pH values.

that further voltage extension is in fact impossible, most likely due to hydrogen evolution on the negative side. Furthermore, the IR drop is more pronounced for the negative electrode, which might suggest that some H₂ molecules are already adsorbed at the surface. The capacitance of the negative electrode slightly increased in comparison to that of the three-electrode cell – 158 F g⁻¹ (63 mAh g⁻¹) here vs. 138 F g⁻¹ (57 mAh g⁻¹) for three-electrode cell; however, one must keep in mind that cyclic voltammetry might reflect different values, depending on the applied scan rate and the experimental configuration. Here, the capacitance might be slightly boosted by the redox response at electrode potential values –0.2 to +0.1 V vs. NHE, most likely reflecting the quinone/hydroquinone redox activity.

The positive electrode capacity is approximately 58 mAh g⁻¹ within 0.3 V potential range; thus, this value is in good accordance with the negative electrode capacitance in the respective potential range (63 mAh g⁻¹).

Electrochemical impedance spectroscopy performed at the open circuit voltage (~0.1 V) within the frequency range of 100 kHz to 1 mHz also confirmed a hybrid charge storage mechanism. The Nyquist plot, presented in Figure 9, reflects at least two semicircles in the high-frequency region. The first one most likely originates from the overall resistance of the system and is reflected as the ohmic drop on the galvanostatic profile. The second one might originate from the redox activity of the bromine-based species, displaying activity on the positive electrode. Diffusion effects, reflected by the sloping profile of the Nyquist spectrum at mid- and low-frequency values, are related to the hindered transport within the porous electrode bulk. Although the PSD (Figure 2) confirmed that the dimensions of the considered ions are still in the range of the pore

diameters in the carbon matrix, one should keep in mind that their mobility within the electrode structure might be severely limited.

The final verification of the system performance concerned long-term cycling. Although the capacitor voltage has been confirmed to be feasible, the cycling stability appeared to be moderate – 80% of the initial capacitance value was reached after 6280 cycles at 1 A g⁻¹. It has been assumed that a lower voltage might considerably improve the long-term performance, as the negative electrode will most likely shift from hydrogen evolution potentials towards higher values. Taking into account the energetic efficiency of the charging/discharging profiles, a maximum capacitor voltage of 1.5 V was selected. With this voltage, the energetic efficiency has been improved by 18%, i.e., from 73% to 89%. The capacitor demonstrated a specific capacitance of 27 F g⁻¹. Taking into account the operating voltage of 1.5 V and discharge time of 30 s, the estimated specific energy density is approximately 8.5 Wh kg⁻¹ and the specific power is 1.1 kW kg⁻¹.

By reducing the operating voltage, the leakage current and self-discharge were diminished; the leakage current decreased to ~10 mA g⁻¹ (vs. 18 mA g⁻¹), and the voltage after 24 hours under open circuit conditions was 0.9 vs. 0.4 V.

3. Summary and Conclusions

Electrochemical capacitors with carbon-based electrodes operating with bromine-based species in electrolytic solutions have been investigated. It seems that for low capacitor voltages (up to 1.2 V), the redox activity of bromides is not observed when Br⁻ is the only component in the electrolytic solution. However, the presence of BrO₃⁻ induces the activity of Br⁻/Br₂/BrO₃⁻ redox couples and enhances the overall capacity.

Notably, the high redox potential of the Br⁻/Br₂ couple (near oxygen evolution potential) might be harmful to the carbon electrode and might induce surface oxidation and further electrode degradation. However, the presence of BrO₃⁻ slightly shifts the redox potential and induces Br₂ generation at lower potentials. As the solubility of Br₂ is higher than that of I₂, the reversibility (e.g., 2Br⁻ ↔ Br₂) is expected (and confirmed) to be satisfactory. *Operando* Raman experiments indicated that there is a covalent interaction between the carbon surface and the Br-based species at higher electrode potentials. This was also confirmed by the XPS profiles. EQCM profiles indicate that these interactions are almost totally reversible. Interestingly, this technique also indicated that the redox activity of bromine-based systems is a multistep and multiproduct process. XPS surveys also indicated that there is a strong affinity of bromides towards the carbon surface, as weak signals have been observed for the initial scans of the surface of the electrode immersed in the electrolytic solutions. Interestingly, it seems that the most problematic issue is not activated carbon ageing but corrosion of the current collectors, as signals for Fe have also been found. This aspect, however, requires further investigation.

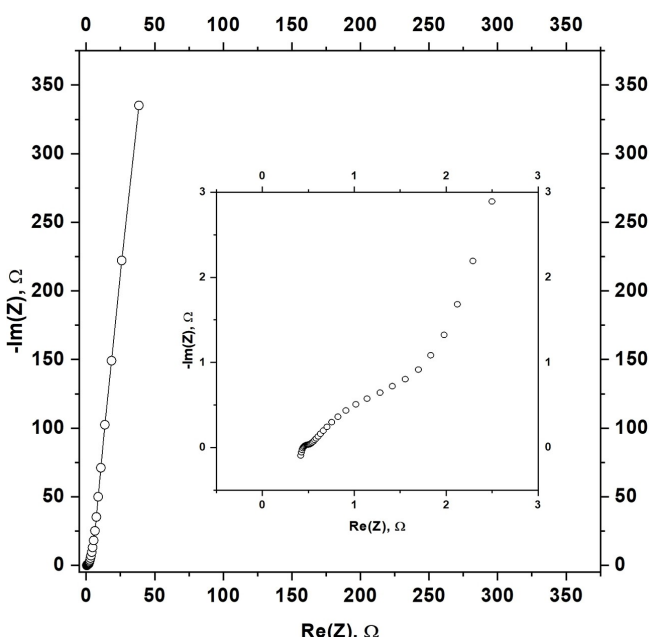


Figure 9. Nyquist plot for the capacitor operating with a 1 mol L⁻¹ KBr + 0.05 mol L⁻¹ KBrO₃ electrolyte at approximately 0.1 V as the open-circuit voltage.

Finally, the metrics of the capacitors operating with bromide-containing aqueous electrolytes appear to be similar to other reported values. The advantage of this system might be seen in the fact that for low capacitor voltages, the performance appears to be typically capacitive. At higher voltages, where the redox activity of $\text{Br}^-/\text{Br}_2/\text{BrO}_3^-$ species is well pronounced, the systems exhibit a higher specific capacitance (and energy) but also suffer from higher leakage currents and more pronounced self-discharge.

Acknowledgements

K.F. would like to express sincere gratitude to all members of the KU Elechem research team, supervised by Prof. Masashi Ishikawa, for their continuous support and help during his research stay at Kansai University. ありがとうございました. K.F. also acknowledges the funding received from the Polish Ministry for Science and Higher Education for research performed at Kansai University (JP) (contract No. 1718/1/MOB/V/2018/0). The European Commission, in the form of The European Research Council, is acknowledged for its financial support within the Starting Grant project (GA 759603) under the European Union's Horizon 2020 Research and Innovation Programme. All authors acknowledge also financial support from Kansai University Graduate School Grant-in-Aid for Promotion of Science and Engineering.

Conflict of Interest

The authors declare no conflict of interest.

Keywords: electrochemical capacitors • redox-active electrolytes • bromide/bromate redox couple • carbon electrode

- [1] P. Simon, Y. Gogotsi, B. Dunn, *Science* **2014**, *343*, 1210.
- [2] K. Naoi, *Electrochemistry* **2013**, *81*, 775–776.
- [3] J. R. Miller, A. F. Burke, *Electrochim. Soc. Interface* **2008**, *17*, 53–57.
- [4] M. Winter, R. J. Brodd, *Chem. Rev.* **2004**, *104*, 4245–4270.
- [5] A. Burke, *J. Power Sources* **2000**, *91*, 37–50.
- [6] Z. Lin, E. Goikolea, A. Balducci, K. Naoi, P. L. Taberna, M. Salanne, G. Yushin, P. Simon, *Mater. Today* **2018**, *21*, 419–436.
- [7] L. Wang, Y. Han, X. Feng, J. Zhou, P. Qi, B. Wang, *Vol. 307*, **2016**, pp. 361–381.
- [8] Y. Zhao, Z. X. Song, X. Li, Q. Sun, N. C. Cheng, S. Lawes, X. L. Sun, *Energy Storage Mater.* **2016**, *2*, 35–62.
- [9] A. Gonzalez, E. Goikolea, J. A. Barrena, R. Mysyk, *Renewable Energy* **2016**, *58*, 1189–1206.
- [10] C. Zhong, Y. Deng, W. Hu, J. Qiao, L. Zhang, J. Zhang, *Chem. Soc. Rev.* **2015**, *44*, 7484–7539.
- [11] F. Beguin, V. Presser, A. Balducci, E. Frackowiak, *Adv. Mater.* **2014**, *26*, 2219–2251, 2283.
- [12] N. Blomquist, T. Wells, B. Andres, J. Backstrom, S. Forsberg, H. Olin, *Sci. Rep.* **2017**, *7*, 39836.
- [13] B. Dyatkin, O. Gogotsi, B. Malinovskiy, Y. Zozulya, P. Simon, Y. Gogotsi, *J. Power Sources* **2016**, *306*, 32–41.
- [14] B. Gorska, E. Frackowiak, F. Beguin, *Curr Opin Electroche* **2018**, *9*, 95–105.
- [15] M. Salanne, *Top. Curr. Chem.* **2017**, *375*, 63.
- [16] A. Balducci, *J. Power Sources* **2016**, *326*, 534–540.
- [17] C. Zhong, Y. Deng, W. Hu, D. Sun, X. Han, J. Qiao, J. Zhang, *Electrolytes for Electrochemical Supercapacitors*, CRC Press, New York, **2016**.
- [18] S. Yamazaki, T. Ito, Y. Murakumo, M. Naitou, T. Shimooka, M. Yamagata, M. Ishikawa, *J. Power Sources* **2016**, *326*, 580–586.
- [19] B. Akinwolewiwa, C. Peng, G. Z. Chen, *J. Electrochim. Soc.* **2015**, *162*, A5054–A5059.
- [20] S. E. Chun, B. Evanko, X. Wang, D. Vonlanthen, X. Ji, G. D. Stucky, S. W. Boettcher, *Nat. Commun.* **2015**, *6*, 7818.
- [21] S. T. Senthilkumar, R. K. Selvan, J. S. Melo, *J. Mater. Chem. A* **2013**, *1*, 12386–12394.
- [22] K. L. Van Aken, M. Beidaghi, Y. Gogotsi, *Angew. Chem. Int. Ed. Engl.* **2015**, *54*, 4806–4809.
- [23] M. He, K. Fic, E. Frackowiak, P. Novák, E. J. Berg, *ChemElectroChem* **2019**, *6*, 566–573.
- [24] M. L. He, K. Fic, E. Frackowiak, P. Novak, E. J. Berg, *Energy Environ. Sci.* **2016**, *9*, 623–633.
- [25] N. Omar, H. Gualous, J. Salminen, G. Mulder, A. Samba, Y. Firouz, M. A. Monem, P. Van den Bossche, J. Van Mierlo, *J. Appl. Electrochem.* **2014**, *44*, 509–522.
- [26] P. Ratajczak, K. Jurewicz, F. Beguin, *J. Appl. Electrochem.* **2014**, *44*, 475–480.
- [27] D. Weingarth, A. Foelske-Schmitz, R. Kötz, *J. Power Sources* **2013**, *225*, 84–88.
- [28] A. Ouakour, B. Tala-Ighil, M. AlSakka, H. Gualous, R. Gallay, B. Boudart, *Electr. Power* **2013**, *95*, 330–338.
- [29] A. M. Bittner, M. Zhu, Y. Yang, H. F. Waibel, M. Konuma, U. Starke, C. J. Weber, *J. Power Sources* **2012**, *203*, 262–273.
- [30] R. German, P. Venet, A. Sari, O. Briat, J. M. Vinassa, in *2012 10th International Power & Energy Conference (IPEC)*, **2012**, pp. 218–223.
- [31] P. Azaïs, L. Duclaux, P. Florian, D. Massiot, M.-A. Lillo-Rodenas, A. Linares-Solano, J.-P. Peres, C. Jehoulet, F. Béguin, *J. Power Sources* **2007**, *171*, 1046–1053.
- [32] O. Bohlen, J. Kowal, D. U. Sauer, *J. Power Sources* **2007**, *172*, 468–475.
- [33] J. C. Icaza, R. K. Guduru, *J. Power Sources* **2016**, *336*, 360–366.
- [34] M. R. Lukatskaya, B. Dunn, Y. Gogotsi, *Nat. Commun.* **2016**, *7*, 12647.
- [35] Y. Dall'Agnese, P. Rozier, P. L. Taberna, Y. Gogotsi, P. Simon, *J. Power Sources* **2016**, *306*, 510–515.
- [36] B. Dyatkin, E. Mamontov, K. M. Cook, Y. Gogotsi, *Prog. Nat. Sci.* **2015**, *25*, 631–641.
- [37] M. D. Levi, M. R. Lukatskaya, S. Sigalov, M. Beidaghi, N. Shpigel, L. Daikhin, D. Aurbach, M. W. Barsoum, Y. Gogotsi, *Adv. Energy Mater.* **2015**, *5*.
- [38] A. Laheer, A. Arenillas, F. Beguin, *J. Power Sources* **2018**, *396*, 220–229.
- [39] B. E. Conway, V. Birss, J. Wojtowicz, *J. Power Sources* **1997**, *66*, 1–14.
- [40] A. Balducci, D. Belanger, T. Brousse, J. W. Long, W. Sugimoto, *J. Electrochim. Soc.* **2017**, *164*, A1487–A1488.
- [41] T. Brousse, D. Bélanger, J. W. Long, *J. Electrochim. Soc.* **2015**, *162*, A5185–A5189.
- [42] T. Shimooka, S. Yamazaki, T. Sugimoto, T. Jyozuka, H. Teraishi, Y. Nagao, H. Oda, Y. Matsuda, M. Ishikawa, *Electrochemistry* **2007**, *75*, 273–279.
- [43] S. Yamazaki, T. Ito, M. Yamagata, M. Ishikawa, *Vol. 41*, *22* ed., **2012**, pp. 15–23.
- [44] S. Yamazaki, T. Ito, M. Yamagata, M. Ishikawa, *Electrochim. Acta* **2012**, *86*, 294–297.
- [45] G. Lota, E. Frackowiak, *Electrochim. Commun.* **2009**, *11*, 87–90.
- [46] G. Lota, K. Fic, E. Frackowiak, *Electrochim. Commun.* **2011**, *13*, 38–41.
- [47] D. J. You, Z. Yin, Y. K. Ahn, S. H. Lee, J. Yoo, Y. S. Kim, *RSC Adv.* **2017**, *7*, 55702–55708.
- [48] H. J. Xie, B. Gelinas, D. Rochefort, *Electrochim. Commun.* **2016**, *66*, 42–45.
- [49] E. Mourad, L. Coustan, S. A. Freunberger, A. Mehdi, A. Vioux, F. Favier, O. Fontaine, *Electrochim. Acta* **2016**, *206*, 513–523.
- [50] S. Sathyamoorthi, M. Kanagaraj, M. Kathiresan, V. Suryanarayanan, D. Velayutham, *J. Mater. Chem. A* **2016**, *4*, 4562–4569.
- [51] Z. J. Zhang, Y. Q. Zhu, X. Y. Chen, Y. Cao, *Electrochim. Acta* **2015**, *176*, 941–948.
- [52] L. B. Chen, Y. R. Chen, J. F. Wu, J. W. Wang, H. Bai, L. Li, *J. Mater. Chem. A* **2014**, *2*, 10526–10531.
- [53] S. T. Senthilkumar, R. K. Selvan, Y. S. Lee, J. S. Melo, *J. Mater. Chem. A* **2013**, *1*, 1086–1095.
- [54] S. Roldán, M. Granda, R. Menéndez, R. Santamaría, C. Blanco, *Electrochim. Acta* **2012**, *83*, 241–246.
- [55] S. Yoshihara, *Electrochemistry* **2016**, *84*, 963–966.
- [56] S. Roldan, C. Blanco, M. Granda, R. Menendez, R. Santamaría, *Angew. Chem. Int. Ed. Engl.* **2011**, *50*, 1699–1701.
- [57] S. Roldan, M. Granda, R. Menendez, R. Santamaría, C. Blanco, *J. Phys. Chem. C* **2011**, *115*, 17606–17611.

- [58] A. Le Comte, D. Chhin, A. Gagnon, R. Retoux, T. Brousse, D. Bélanger, *J. Mater. Chem. A* **2015**, *3*, 6146–6156.
- [59] A. Le Comte, T. Brousse, D. Bélanger, *Electrochim. Acta* **2014**, *137*, 447–453.
- [60] G. Pognon, T. Brousse, L. Demarconnay, D. Belanger, *J. Power Sources* **2011**, *196*, 4117–4122.
- [61] A. Platek, J. Piwek, K. Fic, E. Frackowiak, *Electrochim. Acta* **2019**, *311*, 211–220.
- [62] Q. Li, M. Haque, V. Kuzmenko, N. Ramani, P. Lundgren, A. D. Smith, P. Enoksson, *J. Power Sources* **2017**, *348*, 219–228.
- [63] J. Jagiello, J. P. Olivier, *Adsorption* **2013**, *19*, 777–783.
- [64] J. Jagiello, J. P. Olivier, *Carbon* **2013**, *55*, 70–80.
- [65] A. Laheäär, P. Przygocki, Q. Abbas, F. Béguin, *Electrochim. Commun.* **2015**, *60*, 21–25.
- [66] M. Pourbaix, *Atlas of electrochemical equilibria in aqueous solutions*, 1974.
- [67] K. Xu, *J. Electrochem. Soc.* **1999**, *146*, 4172.
- [68] D. Weingarth, H. Noh, A. Foelske-Schmitz, A. Wokaun, R. Kotz, *Electrochim. Acta* **2013**, *103*, 119–124.
- [69] K. Fic, M. Metier, E. Frackowiak, *J. Electrochem. Soc.* **2015**, *162*, A5140–A5147.
- [70] N. Shpigel, M. R. Lukatskaya, S. Sigalov, C. E. Ren, P. Nayak, M. D. Levi, L. Daikhin, D. Aurbach, Y. Gogotsi, *ACS Energy Lett.* **2017**, *2*, 1407–1415.
- [71] M. D. Levi, S. Sigalov, G. Salitra, R. Elazari, D. Aurbach, *J. Phys. Chem. Lett.* **2011**, *2*, 120–124.
- [72] M. D. Levi, N. Levy, S. Sigalov, G. Salitra, D. Aurbach, J. Maier, *J. Am. Chem. Soc.* **2010**, *132*, 13220–13222.
- [73] M. D. Levi, G. Salitra, N. Levy, D. Aurbach, J. Maier, *Nat. Mater.* **2009**, *8*, 872–875.
- [74] L. J. Hardwick, P. W. Ruch, M. Hahn, W. Scheifele, R. Kötz, P. Novák, *J. Phys. Chem. Solids* **2008**, *69*, 1232–1237.
- [75] M. S. Dresselhaus, A. Jorio, M. Hofmann, G. Dresselhaus, R. Saito, *Nano Lett.* **2010**, *10*, 751–758.
- [76] M. Bouša, O. Frank, I. Jirka, L. Kavan, *physica status solidi (b)* **2013**, *250*, 2662–2667.
- [77] C. T. Chan, K. M. Ho, W. A. Kamitakahara, *Phys. Rev. B* **1987**, *36*, 3499–3502.
- [78] H. Wilhelm, M. Lelaurain, E. McRae, B. Humbert, *J. Appl. Phys.* **1998**, *84*, 6552–6558.
- [79] S. Leyva-Garcia, E. Morallón, D. Cazorla-Amorós, F. Beguin, D. Lozano-Castello, *Carbon* **2014**, *69*, 401–408.
- [80] L. Kavan, L. Dunsch, *ChemPhysChem* **2007**, *8*, 974–998.
- [81] C. Moreno-Castilla, M. V. Lopez-Ramon, F. Carrasco-Marin, *Carbon* **2000**, *38*, 1995–2001.
- [82] A. V. Shchukarev, D. V. Korolkov, *Cent. Eur. J. Chem.* **2004**, *2*, 347–362.

Manuscript received: March 20, 2020

Revised manuscript received: May 3, 2020

Accepted manuscript online: May 25, 2020

Version of record online: June 15, 2020